

Suppression of static ZZ interaction in an all-transmon quantum processor

Peng Zhao,^{1,*} Dong Lan,^{1,†} Peng Xu,² Guangming Xue,³ Mace Blank,¹ Xinsheng Tan,^{1,‡} Haifeng Yu,³ and Yang Yu¹

¹*National Laboratory of Solid State Microstructures, School of Physics, Nanjing University, Nanjing 210093, China*

²*Institute of Quantum Information and Technology, Nanjing University of Posts and Telecommunications, Nanjing, Jiangsu 210003, China*

³*Beijing Academy of Quantum Information Sciences, Beijing 100193, China*

(Dated: December 22, 2024)

The superconducting transmon qubit is currently a leading qubit modality for quantum computing, but gate performance in quantum processor with transmons is often insufficient to support running complex algorithms for practical applications. It is thus highly desirable to further improve gate performance. Due to the weak anharmonicity of transmon, a static ZZ interaction between coupled transmons commonly exists, undermining the gate performance, and in long term, it can become performance limiting. Here we theoretically explore a previously unexplored parameter region in an all-transmon system to address this issue. We show that an feasible parameter region, where the ZZ interaction is heavily suppressed while leaving XY interaction with an adequate strength to implement two-qubit gates, can be found for all-transmon systems. Thus, two-qubit gates, such as cross-resonance gate or iSWAP gate, can be realized without the detrimental effect from static ZZ interaction. To illustrate this, we demonstrate that an iSWAP gate with fast gate speed and dramatically lower conditional phase error can be achieved. Scaling up to large-scale transmon quantum processor, especially the cases with fixed coupling, addressing error, idling error, and crosstalk that arises from static ZZ interaction could also be strongly suppressed.

I. INTRODUCTION

The transmon qubit has been demonstrated as a leading superconducting qubit modality for quantum computing since it has been largely responsible for the recent impressive achievements in superconducting quantum information processing [1–3]. These achievements crucially rely on the improvement of the gate performance through increasing the transmon coherence time [4] and mitigating coherent error from non-ideal parasitic interaction [5–8]. Nonetheless, state-of-the-art gate performance in transmon quantum processor so far is probably insufficient to demonstrate quantum advantage for practical applications [9] and to achieve the long-term goals of fault-tolerant quantum computing [10]. This indicates that considerable effort devoted to improving gate performance is still required.

Despite the benefit of the reproducibly long coherence times, the weak anharmonicity of transmons currently poses a significant challenge to further improve gate performance. For single qubit gates, due to the weak anharmonicity, higher-energy levels of transmon can be easily populated during microwave driven gate operation, causing leakage error. By using the Derivative Removal by Adiabatic Gate (DRAG) scheme [11, 12], this issue can be substantially mitigated without scarifying the gate speed, and single qubit gate with fidelity above 99.9% can be achieved [1, 4]. However, various pending challenges for pursuing two-qubit gates with fast speed and high fidelity still exist due to non-ideal parasitic interactions that arise from the weak anharmonicity of transmons [13, 14]. One of the leading non-ideal parasitic interaction is the static ZZ coupling [15, 16], that has been

shown to undermine the performance of XY interaction based two-qubit gates, such as cross-resonance gate or iSWAP gate [2, 7, 8]. Meanwhile, its residual can cause idling error, and produce quantum crosstalk related to neighboring spectator qubits [17–20]. Hopefully, these idling errors and crosstalk can be strongly suppressed by using a tunable coupler [6, 21–23]. More Recently, it has been demonstrated, both experimentally [24–26] and theoretically [27–29], that this static ZZ can also be suppressed heavily by coupling superconducting qubits with opposite-sign of anharmonicity. However, mitigating static ZZ coupling for XY -based two-qubit gate operations or qubit architecture with fixed inter-qubit coupling is still an outstanding challenge for all-transmon quantum processors [28].

In this work, we show that suppressing static ZZ coupling for two-qubit gate operations can be achieved by engineering quantum interference in an all-transmon quantum processor. Contrary to the commonly accepted view that for all-transmon quantum processors, static ZZ interaction can vanish only by turning off inter-qubit coupling [14, 28]. We find that an experimentally accessible parameter region, where the static ZZ coupling is heavily suppressed while leaving XY interaction with an adequate strength to implement two-qubit gates can be found in an all-transmon system.

II. SYSTEM HAMILTONIAN

Since a superconducting qubit is naturally a multi-level system, especially for qubits with weak anharmonicity such as the transmon, its higher-energy levels have a non-negligible effect on qubit dynamics. For coupled transmons system shown in Fig. 1(a), truncation to the qubit (computational) subspace gives rise an effective two-qubit Hamiltonian with not only an inter-qubit XY coupling J but also a static ZZ coupling ζ that mainly arises from interactions between qubit states and higher-energy states [16, 27]. To suppress this ZZ

*Electronic address: shangniguo@sina.com

†Electronic address: land@nju.edu.cn

‡Electronic address: tanxs@nju.edu.cn

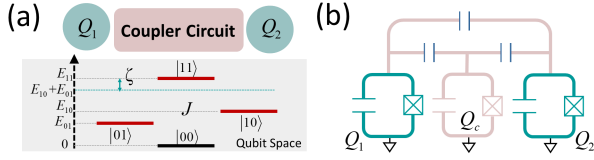


FIG. 1: (a) Circuit layout and level diagram of a coupled two-qubit system. Truncation to qubit space gives rise an effective two-qubit Hamiltonian with an inter-qubit XY coupling J and a static ZZ coupling ζ . (b) Example circuit diagram of two transmons coupled via a coupler circuit combining a capacitor and an ancilla transmon.

coupling for XY -based two qubit gates, here we consider the all-transmon system schematically depicted in Fig. 1(b), where transmons $Q_{1(2)}$ are coupled through a coupling circuit combining an ancilla transmon Q_c and a capacitor. The full system can be modeled by three coupled weakly anharmonic oscillators [30], and described by (hereafter $\hbar = 1$)

$$H = \sum_j (\tilde{\omega}_j q_j^\dagger q_j + \frac{\alpha_j}{2} q_j^\dagger q_j^\dagger q_j q_j) + \sum_{j \neq k} g_{jk} (q_j + q_j^\dagger)(q_k + q_k^\dagger), \quad (1)$$

where subscript $j(k) = \{1, 2, c\}$ labels transmon Q_j with anharmonicity α_j and bare qubit frequency $\tilde{\omega}_j$, q_j (q_j^\dagger) is the associated annihilation (creation) operator, and g_{jk} denotes strength of the coupling between Q_j and Q_k .

We further consider that our system operates in the dispersive regime, i.e., the transmon-coupler detuning $|\Delta_{1(2)}| = |\tilde{\omega}_{1(2)} - \tilde{\omega}_c| \gg g_{1c(2c)}$, and the two transmons are in the straddling regime, i.e., transmon-transmon detuning $|\Delta_{12}| = |\tilde{\omega}_1 - \tilde{\omega}_2| < |\alpha_{1(2)}|$ [23, 31]. Hence, truncation to two-qubit subspace, the Hamiltonian in Eq. (1) can be approximated by an effective two-qubit Hamiltonian

$$H = \omega_1 \frac{ZI}{2} + \omega_2 \frac{IZ}{2} + J \frac{XX + YY}{2} + \zeta \frac{ZZ}{4}, \quad (2)$$

where (X, Y, Z, I) denote the Pauli operators and identity operator, and the order indexes the qubit number, and $\omega_{1(2)}$ represents the dressed qubit frequency of $Q_{1(2)}$. The last two terms corresponds to the XY coupling with strength J and ZZ coupling with strength ζ , respectively. As shown in Fig. 2(a), the XY coupling results from the direct coupling g_{12} and the coupler-mediated indirect coupling, and its strength can be approximated as $J = g_{12} + g_{1c}g_{2c}/\Delta$ with $1/\Delta = (1/\Delta_1 + 1/\Delta_2)/2$ [6, 22]. The ZZ coupling comes from the interaction between qubit states and non-qubit states (including higher-energy states of transmons and coupler states), and its strength is defined as $\zeta = (E_{101} - E_{100}) - (E_{001} - E_{000})$, where E_{mnl} denotes the energy of system eigenstate $|mnl\rangle$ ($m, n, l = \{0, 1, 2\}$), and can be perturbatively obtained [32–35]. Making the rotating-wave approximation (RWA), and deriving up to the fourth-order perturbation gives an approximated expression $\zeta \simeq \zeta_{020} + \zeta_{200} + \zeta_{002} +$

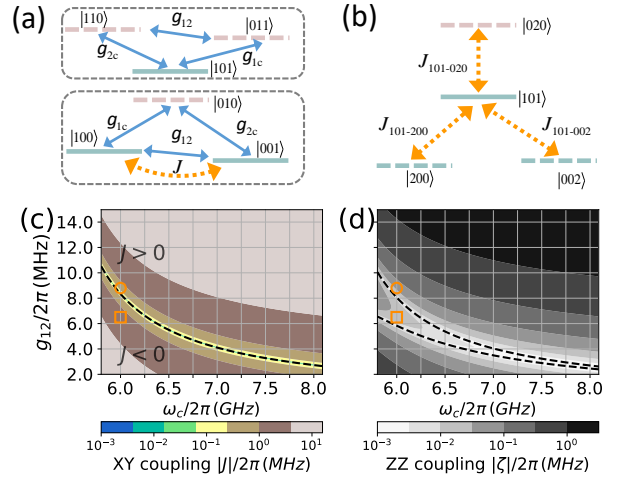


FIG. 2: (a)(b) Level diagram of the coupled transmon system shown in Fig. 1(b). (c) Landscapes of XY coupling J and (d) ZZ coupling ζ (perturbation theory, making RWA) as a function of coupler frequency ω_c and direct coupling strength g_{12} with coupler anharmonicity $\alpha_c = 0$. The dashed curves in (c) and (d) correspond to contours of $J = 0$ and $\zeta = 0$, respectively. The open circle (square) in (c,d) mark the set of parameters chosen to suppress XY (ZZ) coupling.

ζ_1 [32] with

$$\zeta_{020} = \frac{J_{020}^2}{\Delta_1 + \Delta_2 - \alpha_c}, \quad \zeta_{200} = \frac{J_{200}^2}{\Delta_{12} - \alpha_2}, \quad (3)$$

$$\zeta_{002} = -\frac{J_{002}^2}{\Delta_{12} + \alpha_1}, \quad \zeta_1 = \frac{4g_{12}g_{1c}g_{2c}}{\Delta_1\Delta_2},$$

where terms ζ_{020} and $\zeta_{002(200)}$ result from the effective coupling between qubit state $|101\rangle$ and higher-energy states of coupler $|020\rangle$ and transmons $|002(200)\rangle$, respectively, and J_{020} , $J_{200(002)}$ denote the associated effective coupling strength, as shown in Fig. 2(b).

III. SUPPRESSION OF STATIC ZZ INTERACTION FOR OFF-RESONANTLY COUPLED TRANSMONS

First, we consider that transmons are off-resonantly coupled together. According to perturbation analysis [32–35], Figures 2(c) and 2(d) show J and ζ as a function of coupler frequency ω_c and direct coupling strength g_{12} with $\tilde{\omega}_{1(2)}/2\pi = 5.114$ (4.914) GHz, $\alpha_{1(2)}/2\pi = -330$ MHz, $\alpha_c/2\pi = 0$ MHz (linear coupler), and $g_{1c(2c)}/2\pi = 98$ (83) MHz [7, 36]. One can find that in the parameter space of (ω_c, g_{12}) , zero-point for XY coupling forms a single branch (dashed line in Fig. 2(c)), and when the coupler has larger transition frequency, the zero- ZZ regime almost overlap with the zero- XY branch, conforming the commonly accepted view, i.e., static ZZ interaction can be suppressed by turning off inter-qubit coupling. However, interestingly and unexpectedly, with decreasing the coupler frequency, the

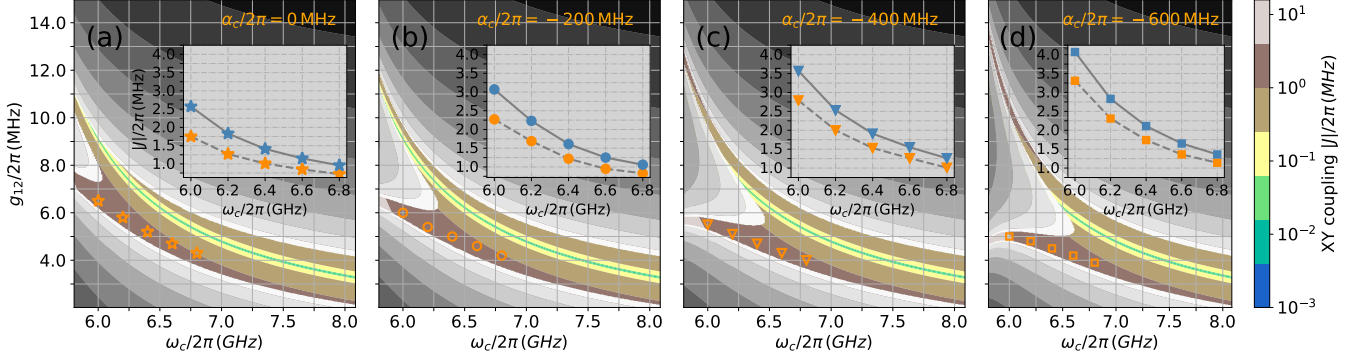


FIG. 3: Landscapes of XY coupling J (perturbation theory, without making RWA) and ZZ coupling ζ (numerical diagonalization) as a function of coupler frequency ω_c and direct coupling strength g_{12} with coupler anharmonicity (a) $\alpha_c/2\pi = 0$ (linear coupler), (b) $\alpha_c/2\pi = -200$ MHz, (c) $\alpha_c/2\pi = -400$ MHz, and (d) $\alpha_c/2\pi = -600$ MHz. The other system parameters are similar to those used in Fig. 2. For each coupler anharmonicity, the two landscapes are shown in single panel, and the data point in the landscape of ZZ coupling with ζ below 20 KHz is removed. The Insets of (a-d) show the maintained XY coupling strength obtained with the corresponding parameter set marked in (a-d). The solid (dashed) line represents the result derived from perturbation theory (the period T of the simulated cross-resonance oscillation).

zero- ZZ regime gradually diverging and eventually splitting into two separate branches (dashed lines in Fig. 2(d)), and the presence of the lower branch shows that ZZ coupling can be heavily suppressed without the need for suppressing XY coupling, thus one can mitigate static ZZ coupling for implementing XY -based two-qubit gates.

The physics behind the above interesting features are: (i) As shown in Eq. (3), when coupler has larger transition frequency, the energy of coupler state $|020\rangle$ is far larger than that of the states $|101\rangle$ and $|200(002)\rangle$, i.e., $E_{020} \gg \{E_{101}, E_{200}, E_{002}\}$, and $\Delta_{1(2)} \gg \{\Delta_{12}, \alpha_{1(2)}\}$, the terms ζ_{020} and ζ_1 can be omitted. Thus, the dominated contribution to the total ZZ coupling results from the effective interaction between qubit state $|101\rangle$ and higher-energy states $|200\rangle$ ($|002\rangle$), whose strength can be approximated as $J_{200(002)} \sim \sqrt{2}J$ [32]. When the inter-qubit XY coupling J is tuned off, the interactions between $|101\rangle$ and $|200\rangle$ ($|002\rangle$) are also turned off effectively, causing suppression of ZZ coupling.

(ii) However, when decreasing the coupler frequency, thus $E_{020} \gtrsim \{E_{101}, E_{200}, E_{002}\}$ and $\Delta_{1(2)} \gtrsim \{\Delta_{12}, \alpha_{1(2)}\}$, the terms ζ_{020} and ζ_1 can no longer be neglected. Since $E_{020} > E_{101} > \{E_{200}, E_{002}\}$, the interaction $|101\rangle \leftrightarrow |200\rangle$ ($|002\rangle$) gives rise an ZZ coupling term with a positive sign, while the interaction $|101\rangle \leftrightarrow |020\rangle$ contributes a term with a negative sign. Therefore, the conditions for suppressing ZZ coupling cannot be achieved by just turning off the XY coupling. To the opposite, the XY coupling should be tuned on, thus the positive contribution and the negative contribution can interfere destructively, giving rise the suppression of net ZZ coupling. Moreover, since $\zeta_{200(002)} \propto (\sqrt{2}J)^2$ [32], for a fixed coupler frequency, there should be two different values of g_{12} (giving rise a total XY coupling of same magnitude but opposite signs) for suppressing ZZ coupling. Up to now, the discussion above suggests that the zero- ZZ regime should be split into two separate branches which are approximately symmetrical with respect to the zero- XY branch. Thus for a

given coupler frequency, the strength of the maintained XY coupling in the lower and upper branch of the zero- ZZ region should be approximately equal. However, as shown in Eq. (3), along with the terms associated with higher-energy state of transmons and coupler, there is an addition terms ζ_1 associated with lower-energy states giving rise a positive contribution with strength $\zeta_1 \propto g_{12}$. Thus, taking all these terms in Eq. (3) into consideration, the strength of the maintained XY coupling in the lower branch should be larger than that in the upper branch, as shown in Fig. 2(d).

To numerically verify the above results, we consider two sets of parameters, i.e., (6.0, 6.5) and (6.0, 8.8), which are chosen to suppress XY and ZZ coupling, respectively. The ZZ coupling strength can be exactly obtained by numerical diagonalization of the system Hamiltonian in Eq. (1), giving rise $|\zeta|/2\pi = 3.9$ (3.3) KHz for the two parameter sets. while for XY coupling, we note that the effective XY coupling is not perfectly well-defined for present system with off-resonantly coupled transmons. Here the XY coupling strength is estimated from the period T of the simulated cross-resonance oscillation with the controlled qubit Q_1 in its ground state [32]. In the weak-drive limit, the period T can be well approximated by $2\pi/T = J\Omega_d/\Delta_{12}$ [36], where Ω_d denotes strength of the driving applied on Q_1 . As such, the estimated XY coupling strength are $J/2\pi = 1.75$ (0.63) MHz.

The above numerical results confirm that for systems operating on the lower branch of zero- ZZ region, the ZZ coupling can indeed be strongly suppressed without the need for suppressing the XY coupling heavily. However, the maintained XY coupling (here is 1.75 MHz) is too weak to support implementing a successful two-qubit gate, such as the cross-resonance gate [37]. To achieve a larger maintained XY coupling for a given coupler frequency, according to the above analysis, one can reduce the energy of $|020\rangle$ by replacing the linear coupler ($\alpha_c = 0$) with a nonlinear coupler with $\alpha_c < 0$, such as a transmon. Then the negative ZZ contribution (ζ_{020})

from interaction $|101\rangle \leftrightarrow |020\rangle$ gets larger, and a larger XY coupling J is thus needed to suppress ZZ coupling. Figure 3 show the numerical calculated ZZ coupling strength and the XY coupling strength as a function of ω_c and g_{12} with coupler anharmonicity $\alpha_c/2\pi = \{0, -200, -400, -600\}$ MHz. The other parameters are same to those used in Fig. 2. In order to easily identify the desired parameter region for suppressing ZZ coupling, for each coupler anharmonicity, the associated two landscapes (XY and ZZ where date point with ZZ coupling strength below 20 KHz is removed) are shown in a single panel. One can find that the lower branch of zero- ZZ region is shifted downward along with the increased coupler anharmonicity. Thus, the maintained XY coupling is also increased, as shown in the inset of Fig. 3. Thus, by using the transmon coupler, the static ZZ coupling below 20 KHz and the maintained XY coupling strength above 2 MHz should be assessed experimentally for implementing cross-resonance gate with current fabrication technology [38, 39]. We note that the maintained XY coupling may further increase by optimizing the full system parameters [32].

IV. SUPPRESSION OF STATIC ZZ INTERACTION FOR ON-RESONANTLY COUPLED TRANSMONS

Having shown the suppression of ZZ coupling for the off-resonantly coupled case, we now turn to consider the on-resonance case. Fig. 4(a) shows the numerically calculated ZZ coupling strength ζ and XY coupling strength J (extracted as half the energy difference between the eigenstate $|100\rangle$ and $|001\rangle$) as a function of ω_c and g_{12} for resonantly coupled transmons. Similar to that of the off-resonantly coupled case, here, the zero- ZZ points also form two branches in the parameter space (ω_c, g_{12}) [32], where the lower branches allow us to mitigate ZZ coupling for on-resonance XY coupling based two-qubit gates.

To illustrate this, we consider the implementation of an iSWAP gate with diabatic scheme [15, 40], and in order to mitigate leakage, here the direct coupling strength g_{12} are chosen to achieve the full synchronization between the swap and leakage error channels [40]. During the gate operations, the frequency of the transmon Q_1 stays fixed at 6.50 GHz, while the frequencies of coupler Q_c and transmon Q_2 vary from their idle point ($\omega_{c(2)}/2\pi = 8.70$ (6.45) GHz, where both XY and ZZ coupling are strongly suppressed) to their interaction point and then come back according to the Gaussian flat-top pulse with a fixed rise/fall time of 5.66 ns [41]. We firstly consider that the system operates in the dispersive regime, and coupler interaction frequency takes $\omega_c/2\pi \approx 7.79$ GHz, marked by the open square in Fig. 4(a), and the associated control pulse is shown as the dashed line in Fig. 4(b). Fig. 4(c) shows the swap error $\varepsilon_{\text{swap}} = 1 - P_{001}$ (P_{001} denotes the population in $|001\rangle$ after the time evolution for system initialized in $|100\rangle$) and the leakage L_1 [42, 43] as function of the hold time that is defined as the time-interval between the midpoints of the ramps [40]. One can find that an iSWAP gate with an intrinsic gate fidelity [44] of 99.994% and leakage L_1 below 0.006% can be achieved with a hold time of 57 ns. More-

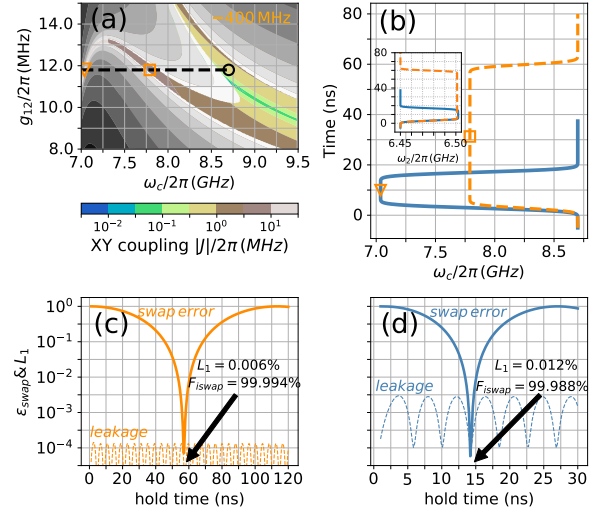


FIG. 4: (a) Landscapes of numerically calculated XY coupling strength J and ZZ coupling strength ζ (date point with ZZ coupling strength below 20 KHz is removed) as a function of coupler frequency ω_c and direct coupling strength g_{12} in the two-transmon system (Fig. 1(b)) with qubit frequency $\omega_{1(2)}/2\pi = 6.5$ GHz, qubit anharmonicity $\alpha_{1(2)}/2\pi = -250$ MHz, coupler anharmonicity $\alpha_c/2\pi = -400$ MHz, and frequency-dependent transmon-coupler coupling strength $g_{1c(2c)}/2\pi = 125\sqrt{\omega_c/\omega_1}$ ($130\sqrt{\omega_c/\omega_2}$) MHz [40]. The parameter set marked by an open circle denotes the idling frequency point for the coupler, and the dashed line indicates the direct coupling strength adopted for mitigating the leakage during the iSWAP gate operation. (b) Typical control pulse for implementing an iSWAP gate, where the full width at half maximum is defined as hold time. The dashed (solid) line shows the control pulse for system operated in dispersive (quasi-dispersive) regime, marked by the open square (triangle) in (a). (c), (d) Swap error $\varepsilon_{\text{swap}}$ and leakage L_1 as a function of hold time with system operated in dispersive regime and quasi-dispersive regime, respectively.

over, by extracting conditional phase error δ_θ , we find that δ_θ is suppressed below 0.001 rad, comforting strong suppression of ZZ coupling. In Fig. 4(d), we also show the result for the system operated in the quasi-dispersive regime [45, 46], and the control pulse is shown as the solid line in Fig. 4(b), where $\omega_c/2\pi \approx 7.04$ GHz (also marked by the open circle in Fig. 4(a)), giving the $g_{1c(2c)}/\Delta_{1(2)} \approx 1/4$. Although operating in the quasi-dispersive regime, an iSWAP gate with fidelity above 99.988% and leakage L_1 below 0.012% can still be achieved with a hold time of 14.3 ns. The extracted conditional phase error is suppressed below 0.003 rad.

V. CONCLUSION

In summary, we have demonstrated that a feasible parameter region, where static ZZ coupling is heavily suppressed while leaving XY interaction with an adequate strength to implement two-qubit gates, such as cross-resonance gate or iSWAP gate, can be found in an all-transmon system. We

further show that an iSWAP gate with fast gate speed and dramatically low conditional phase error can indeed be achieved in this parameter region. Without the detrimental effect from the static ZZ coupling, for transmon quantum processor with fixed coupling, single-qubit addressing error, idling error, and crosstalk that arise from static ZZ coupling should also be heavily suppressed. From the point view of perturbation theory, the main physics behind these benefits is that in the proposed system, XY and ZZ coupling are enabled by different virtual transitions and different intermediate states, thus providing the possibility to engineer quantum interference for mitigating ZZ coupling while retaining XY coupling. One thus reasonably estimate that it is also possible to achieve the mitigation of static ZZ coupling for XY -based two-qubit gates with other types of coupler circuits [23, 32].

Recently, we became aware of related experimental work on suppression of ZZ interactions for all-transmon qubit systems in Refs.[47, 48].

Acknowledgments

We thank Ji Chu for insightful discussion. This work was partly supported by the National Key Research and Development Program of China (Grant No.2016YFA0301802), the National Natural Science Foundation of China (Grant No.61521001, and No.11890704), and the Key R&D Program of Guangdong Province (Grant No.2018B030326001). X. T. acknowledges the supported by the National Natural Science Foundation of China (Grant No.12074179). P. X. acknowledges the supported by the Young fund of Jiangsu Natural Science Foundation of China (Grant No.BK20180750). H. Y. acknowledges support from the Beijing Natural Science Foundation (Grant No.Z190012).

P. Z. and D. L. contributed equally to this work.

-
- [1] R. Barends, J. Kelly, A. Megrant, A. Veitia, D. Sank, E. Jeffrey, T. C. White, J. Mutus, A. G. Fowler, B. Campbell, Y. Chen, Z. Chen, B. Chiaro, A. Dunsworth, C. Neill, P. O'Malley, P. Roushan, A. Vainsencher, J. Wenner, A. N. Korotkov, A. N. Cleland, and J. M. Martinis, Superconducting quantum circuits at the surface code threshold for fault tolerance, *Nature* **508**, 500 (2014).
- [2] F. Arute, K. Arya, R. Babbush, D. Bacon, J. C. Bardin, R. Barends, R. Biswas, S. Boixo, F. G. Brandao, D. A. Buell *et al.*, Quantum supremacy using a programmable superconducting processor, *Nature* **574**, 505 (2019).
- [3] P. Jurcevic, A. Javadi-Abhari, L. S. Bishop, I. Lauer, D. F. Bogorin *et al.*, Demonstration of quantum volume 64 on a superconducting quantum computing system, *Quantum Sci. Technol.* **6**, 025020 (2021).
- [4] M. Kjaergaard, M. E. Schwartz, J. Braumüller, P. Krantz, J. I.-J. Wang, S. Gustavsson, and W. D. Oliver, Superconducting qubits: Current state of play, *arXiv:1905.13641* (2019).
- [5] J. M. Martinis and M. R. Geller, Fast adiabatic qubit gates using only σ^z control, *Phys. Rev. A* **90**, 022307 (2014)
- [6] F. Yan, P. Krantz, Y. Sung, M. Kjaergaard, D. L. Campbell, T. P. Orlando, S. Gustavsson, and W. D. Oliver, Tunable Coupling Scheme for Implementing High-Fidelity Two-Qubit Gates, *Phys. Rev. Applied* **10**, 054062 (2018).
- [7] S. Sheldon, E. Magesan, J. M. Chow, and J. M. Gambetta, Procedure for systematically tuning up cross-talk in the cross-resonance gate, *Phys. Rev. A* **93**, 060302(R) (2016).
- [8] N. Sundaresan, I. Lauer, E. Pritchett, E. Magesan, P. Jurcevic, and J. M. Gambetta, Reducing unitary and spectator errors in cross resonance with optimized rotary echoes, *arXiv:2007.02925*.
- [9] J. Preskill, Quantum Computing in the NISQ era and beyond, *Quantum* **2**, 79 (2018).
- [10] A. G. Fowler, M. Mariantoni, J. M. Martinis, and A. N. Cleland, Surface codes: Towards practical large-scale quantum computation, *Phys. Rev. A* **86**, 032324 (2012).
- [11] F. Motzoi, J. M. Gambetta, P. Rebentrost, and F. K. Wilhelm, Simple Pulses for Elimination of Leakage in Weakly Nonlinear Qubits, *Phys. Rev. Lett.* **103**, 110501 (2009)
- [12] Z. Chen, J. Kelly, C. Quintana, R. Barends, B. Campbell, Y. Chen, B. Chiaro, A. Dunsworth, A. G. Fowler, E. Lucero, E. Jeffrey, A. Megrant, J. Mutus, M. Neeley, C. Neill, P. J. J. ÓMalley, P. Roushan, D. Sank, A. Vainsencher, J. Wenner, T. C. White, M. R. Jeffrey, A. Megrant, J. Mutus, M. Neeley, C. Neill, P. J. J. ÓMalley, P. Roushan, D. Sank, A. Vainsencher, J. Wenner, T. C. White, A. N. Korotkov, and J. M. Martinis, Measuring and Suppressing Quantum State Leakage in a Superconducting Qubit, *Phys. Rev. Lett.* **116**, 020501 (2016)
- [13] P. Krantz, M. Kjaergaard, F. Yan, T. P. Orlando, S. Gustavsson, and W. D. Oliver, A quantum engineer's guide to superconducting qubits, *Applied Physics Reviews* **6**, 021318 (2019).
- [14] A. Blais, A.L. Grimsmo, S.M. Girvin and A. Wallraff, Circuit Quantum Electrodynamics, *arXiv:2005.12667*.
- [15] F. W. Strauch, P. R. Johnson, A. J. Dragt, C. J. Lobb, J. R. Anderson, and F. C. Wellstood, Quantum Logic Gates for Coupled Superconducting Phase Qubits, *Phys. Rev. Lett.* **91**, 167005 (2003).
- [16] L. DiCarlo, J. M. Chow, J. M. Gambetta, L. S. Bishop, B. R. Johnson, D. I. Schuster, J. Majer, A. Blais, L. Frunzio, S. M. Girvin, and R. J. Schoelkopf, Demonstration of two-qubit algorithms with a superconducting quantum processor, *Nature (London)* **460**, 240 (2009).
- [17] D. C. McKay, S. Sheldon, J. A. Smolin, J. M. Chow, and J. M. Gambetta, Three Qubit Randomized Benchmarking, *Phys. Rev. Lett.* **122**, 200502 (2019).
- [18] M. Takita, A. D. Córcoles, E. Magesan, B. Abdo, M. Brink, A. Cross, J. M. Chow, and J. M. Gambetta, Demonstration of Weight-Four Parity Measurements in the Surface Code Architecture, *Phys. Rev. Lett.* **117**, 210505 (2016).
- [19] C. C. Bultink, T. E. O'Brien, R. Vollmer, N. Muthusubramanian, M. W. Beekman, M. A. Rol, X. Fu, B. Tarasinski, V. Ostroukh, B. Varbanov, A. Bruno, and L. DiCarlo, Protecting quantum entanglement from qubit errors and leakage via repetitive parity measurements, *arXiv:1905.12731* (2020).
- [20] S. Krinner, S. Lazar, A. Remm, C.K. Andersen, N. Lacroix, G.J. Norris, C. Hellings, M. Gabureac, C. Eichler, and A. Wallraff, Benchmarking Coherent Errors in Controlled-Phase Gates due to Spectator Qubits, *Phys. Rev. Applied* **14**, 024042 (2020).
- [21] Y. Chen, C. Neill, P. Roushan, N. Leung, M. Fang, R. Barends, J. Kelly, B. Campbell, Z. Chen, B. Chiaro, A. Dunsworth, E. Jeffrey, A. Megrant, J. Y. Mutus, P. J. J. O'Malley, C. M. Quintana, D. Sank, A. Vainsencher, J. Wenner, T. C. White, M. R.

- Geller, A. N. Cleland, and J. M. Martinis, Qubit architecture with high coherence and fast tunable coupling, *Phys. Rev. Lett.* **113**, 220502 (2014).
- [22] C. Neill. A path towards quantum supremacy with superconducting qubits. PhD thesis, University of California Santa Barbara, Dec 2017.
- [23] P. S. Mundada, G. Zhang, T. Hazard, and A. A. Houck, Suppression of Qubit Crosstalk in a Tunable Coupling Superconducting Circuit, *Phys. Rev. Applied* **12**, 054023 (2019).
- [24] J. Ku, X. Xu, M. Brink, D. C. McKay, J. B. Hertzberg, M. H. Ansari, and B. L. T. Plourde, Suppression of Unwanted ZZ Interactions in a Hybrid Two-Qubit System, *Phys. Rev. Lett.* **125**, 200504 (2020).
- [25] R. Winik, C. Leroux, A. D. Paolo, T. Hazard, R. Shillito, A. Vepsäläinen, Y. Sung, Z. Ao, M. Kjaergaard, J. Braumueller, M. Schwartz, K. Serniak, D. K. Kim, J. Yoder, A. Melville, B. Niedzielski, A. Blais, S. Gustavsson, and W. Oliver, Cancellation of unwanted ZZ interactions for cross-resonance gates by superconducting qubit engineering, Bulletin of the American Physical Society, 2021.
- [26] K. Zuo, Y. Urade, Z. Yan, S. Tamate, Y. Tabuchi, H. Terai, and Y. Nakamura, Inductively shunted transmon qubit for ZZ interaction cancellation, Bulletin of the American Physical Society, 2021.
- [27] P. Zhao, P. Xu, D. Lan, J. Chu, X. Tan, H. Yu, and Y. Yu, High-Contrast ZZ Interaction Using Superconducting Qubits with Opposite-Sign Anharmonicity, *Phys. Rev. Lett.* **125**, 200503 (2020).
- [28] X. Xu and M.H. Ansari, ZZ freedom in two qubit gates, [arXiv:2009.00485](https://arxiv.org/abs/2009.00485).
- [29] P. Zhao, P. Xu, D. Lan, X. Tan, H. Yu, and Y. Yu, Switchable Next-Nearest-Neighbor Coupling for Controlled Two-Qubit Operations, *Phys. Rev. Applied* **14**, 064016 (2020).
- [30] J. Koch, T. M. Yu, J. Gambetta, A. A. Houck, D. I. Schuster, J. Majer, A. Blais, M. H. Devoret, S. M. Girvin, and R. J. Schoelkopf, Charge-insensitive qubit design derived from the cooper pair box, *Phys. Rev. A* **76**, 042319 (2007).
- [31] In present work, our discussion is restricted on all-transmon system where qubits are in the straddling regime. For transmons out of straddling regime, the previous numerical result does not show any possibility for achieving suppression of static ZZ coupling in all-transmon device operated in a reasonable coupling regime [23].
- [32] See Supplemental Material for further details.
- [33] R. Krishnan and J. A. Pople, Approximate fourth-order perturbation theory of the electron correlation energy, *Int. J. Quantum Chem.* **14**, 91 (1978).
- [34] X. Li, T. Cai, H. Yan, Z. Wang, X. Pan, Y. Ma, W. Cai, J. Han, Z. Hua, X. Han, Y. Wu, H. Zhang, H. Wang, Yipu Song, Luming Duan, and Luyan Sun, Tunable Coupler for Realizing a Controlled-Phase Gate with Dynamically Decoupled Regime in a Superconducting Circuit, *Phys. Rev. Applied* **14**, 024070 (2020).
- [35] J. Chu *et al.*, in preparation. (2020).
- [36] E. Magesan and J. M. Gambetta, Effective Hamiltonian models of the cross-resonance gate, *Phys. Rev. A* **101**, 052308 (2020).
- [37] F. Solgun, D. DiVincenzo, and J. Gambetta, Simple Impedance Response Formulas for the Dispersive Interaction Rates in the Effective Hamiltonians of Low Anharmonicity Superconducting Qubits, *IEEE Trans. Microw. Theory Tech.* **67**, 928 (2019).
- [38] J. M. Kreikebaum, K. P. O'Brien, A. Morvan, and I. Siddiqi, Improving wafer-scale Josephson junction resistance variation in superconducting quantum coherent circuits, *Supercond. Sci. Technol.* **33**, 06LT02 (2020).
- [39] J. B. Hertzberg, E. J. Zhang, S. Rosenblatt, E. Magesan, J. A. Smolin, J.-B. Yau, V. P. Adiga, M. Sandberg, M. Brink, J. M. Chow, and J. S. Orcutt, Laser-annealing Josephson junctions for yielding scaled-up superconducting quantum processors, [arXiv:2009.00781](https://arxiv.org/abs/2009.00781).
- [40] R. Barends, C. M. Quintana, A. G. Petukhov, Y. Chen, D. Kafri, K. Kechedzhi *et al.*, Diabatic Gates for Frequency-Tunable Superconducting Qubits, *Phys. Rev. Lett.* **123**, 210501 (2019).
- [41] J. Ghosh, A. Galiatdinov, Z. Zhou, A. N. Korotkov, J. M. Martinis, and M. R. Geller, High-fidelity controlled- σ^z gate for resonator-based superconducting quantum computers, *Phys. Rev. A* **87**, 022309 (2013).
- [42] C. J. Wood and J. M. Gambetta, Quantification and characterization of leakage errors, *Phys. Rev. A* **97**, 032306 (2018).
- [43] M. A. Rol, F. Battistel, F. K. Malinowski, C. C. Bultink, B. M. Tarasinski, R. Vollmer, N. Haider, N. Muthusubramanian, A. Bruno, B. M. Terhal, and L. DiCarlo, Fast, High-Fidelity Conditional-Phase Gate Exploiting Leakage Interference in Weakly Anharmonic Superconducting Qubits, *Phys. Rev. Lett.* **123**, 120502 (2019).
- [44] L. H. Pedersen, N. M. Møller, and K. Mølmer, Fidelity of quantum operations, *Phys. Lett. A* **367**, 47 (2007).
- [45] M. H. Goerz, F. Motzoi, K. B. Whaley, and C. P. Koch, Charting the circuit QED design landscape using optimal control theory, *npj Quantum Information* **3**, 37 (2017).
- [46] It is worth noting that in a system comprising two fixed-frequency transmons that are coupled via a bus resonator, M. H. Goerz *et al.* [45] have theoretically explored a similar parameter regime (which has been nicknamed 'Quasi-Dispersive Straddling Qubits (QuaDiSQ) regime'), where the residual static ZZ coupling is heavily suppressed, while all-microwave controlled entanglement gates can still be achieved. In this case, the ZZ coupling is mainly resulted from the interaction between qubit state $|101\rangle$ and higher-energy state $|200(002)\rangle$ (giving a positive contribution) and $|020\rangle$ (giving a negative contribution) [16]. Thus for system operated in QuaDiSQ regime, the positive and negative contribution can destructive interference, eliminating the residual ZZ interaction. For qubit architecture with tunable coupler, as shown in Fig. 4(a), when system operates in quasi-dispersive regime and two transmons are on resonance (in straddling regime), similar results can also be obtained for system with smaller direct coupling strength, i.e., the static ZZ interaction is eliminated, while larger XY coupling is still preserved.
- [47] Y. Sung, L. Ding, J. Braumüller, A. Vepsäläinen, B. Kannan, M. Kjaergaard, A. Greene, G. O. Samach, C. McNally, D. Kim, A. Melville, B. M. Niedzielski, M. E. Schwartz, J. L. Yoder, T. P. Orlando, S. Gustavsson, and W. D. Oliver, Realization of high-fidelity CZ and ZZ-free iSWAP gates with a tunable coupler, [arXiv:2011.01261](https://arxiv.org/abs/2011.01261).
- [48] A. Kandala, K. X. Wei, S. Srinivasan, E. Magesan, S. Carnevale, G. A. Keefe, D. Klaus, O. Dial, and D. C. McKay, Demonstration of a High-Fidelity CNOT for Fixed-Frequency Transmons with Engineered ZZ Suppression, [arXiv:2011.07050](https://arxiv.org/abs/2011.07050).

Supplementary information for "Suppression of static ZZ interaction in an all-transmon quantum processor"

Peng Zhao,^{1,*} Dong Lan,^{1,†} Peng Xu,² Guangming Xue,³ Mace Blank,¹ Xinsheng Tan,^{1,‡} Haifeng Yu,³ and Yang Yu¹

¹National Laboratory of Solid State Microstructures, School of Physics, Nanjing University, Nanjing 210093, China

²Institute of Quantum Information and Technology, Nanjing University of Posts and Telecommunications, Nanjing, Jiangsu 210003, China

³Beijing Academy of Quantum Information Sciences, Beijing 100193, China

(Dated: May 12, 2021)

STRENGTH OF STATIC ZZ COUPLING

In this section, according to perturbation theory [1], we present the details deviation of the static ZZ coupling strength ζ for our two-transmon system. In order to give a clear explanation of how to mitigating ZZ coupling for XY-based gate operations, in the following discussion, we have made two approximations: (i) Making the rotating-wave approximation (RWA) by neglecting the counter-rotating terms in Eq. (1) of the main text, the system Hamiltonian now reads $H = H_0 + V$, with

$$H_0 = \sum_j \left[\tilde{\omega}_j q_j^\dagger q_j + \frac{\alpha_j}{2} q_j^\dagger q_j^\dagger q_j q_j \right], \quad (1)$$

$$V = \sum_{j,k} g_{jk} (q_j^\dagger q_k + q_j q_k^\dagger),$$

and its level diagram is shown in Fig. 1. (ii) Since $g_{12} \ll \{g_{1c}, g_{2c}\}$ and $\Delta_{1(2)} \gg \{\Delta_{12}, \alpha_{1,2,c}\}$, one can neglect small terms in the calculation of ZZ coupling strength ζ .

The perturbed result for ZZ coupling strength ζ can be defined as $\zeta \equiv \zeta^{(2)} + \zeta^{(3)} + \zeta^{(4)}$, where $\zeta^{(n)}$ denotes n th-order perturbational result, defined as $\zeta^{(n)} \equiv (E_{101}^{(n)} - E_{001}^{(n)}) -$

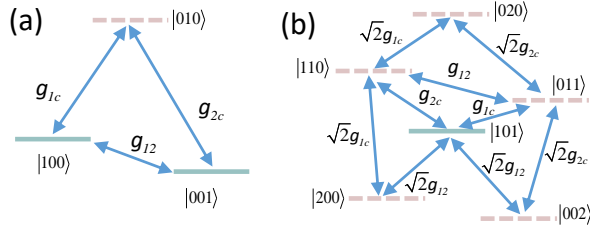


FIG. 1: Level diagram of the coupled transmon system. (a) one-excitation subspace. (b) two-excitation subspace. The green solid lines denote qubit level, while the pink dashed lines represent the non-qubit levels.

$(E_{100}^{(n)} - E_{000}^{(n)})$ with

$$E_s^{(2)} = \sum_{j \neq s} \frac{|V_{sj}|^2}{E_{sj}},$$

$$E_s^{(3)} = \sum_{j,k \neq s} \frac{V_{sj} V_{jk} V_{ks}}{E_{sj} E_{sk}}, \quad (2)$$

$$E_s^{(4)} = \sum_{j,k,l \neq s} \frac{V_{sj} V_{jk} V_{kl} V_{ls}}{E_{sj} E_{sk} E_{sl}} + \sum_{j,k \neq s} \frac{|V_{sj}|^2 |V_{sk}|^2}{E_{sj}^2 E_{sk}},$$

where $V_{sj} = \langle s|V|j \rangle$ and $E_{sj} = E_s^{(0)} - E_j^{(0)}$. Thus, after making the above mentioned two approximations, and according to the expression in Eq. (2), one has [1–3]

$$\zeta^{(2)} = 2g_{12}^2 \left[\frac{1}{\Delta_{12} - \alpha_2} - \frac{1}{\Delta_{12} + \alpha_1} \right], \quad (3)$$

$$\zeta^{(3)} = 2g_{12}g_{1c}g_{2c} \left[\frac{2}{(\Delta_{12} - \alpha_2)\Delta_1} - \frac{2}{(\Delta_{12} + \alpha_1)\Delta_2} + \frac{2}{\Delta_1\Delta_2} \right], \quad (4)$$

$$\zeta^{(4)} = 2g_{1c}^2g_{2c}^2 \left[\frac{1}{\Delta_1^2(\Delta_{12} - \alpha_2)} - \frac{1}{\Delta_2^2(\Delta_{12} + \alpha_1)} + \frac{1}{\Delta_1 + \Delta_2 - \alpha_c} \left(\frac{1}{\Delta_1} + \frac{1}{\Delta_2} \right)^2 \right]. \quad (5)$$

To identify the physical mechanism behind these terms ($\zeta^{(2)}, \zeta^{(3)}, \zeta^{(4)}$), and also to give a clear analysis of the relation between ZZ coupling strength ζ and XY coupling strength J , after writing out all these terms and rearranging them, ζ can be approximated as (here we recover the Eq. (3) of the main text)

$$\zeta \simeq \zeta_{020} + \zeta_{200} + \zeta_{002} + \zeta_1,$$

$$\zeta_{020} = \frac{J_{020}^2}{\Delta_1 + \Delta_2 - \alpha_c}, \quad \zeta_{200} = \frac{J_{200}^2}{\Delta_{12} - \alpha_2}, \quad (6)$$

$$\zeta_{002} = -\frac{J_{002}^2}{\Delta_{12} + \alpha_1}, \quad \zeta_1 = \frac{4g_{12}g_{1c}g_{2c}}{\Delta_1\Delta_2},$$

where terms $\zeta_{020} \zeta_{002(200)}$ can be considered as the ZZ contributions resulting from the effective coupling between qubit state $|101\rangle$ and higher-energy states of coupler $|020\rangle$ and

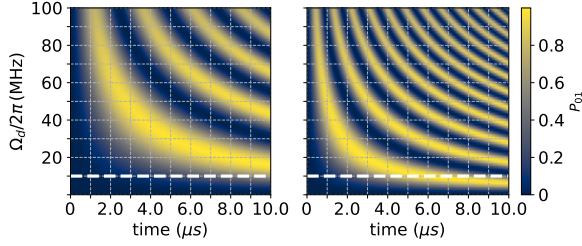


FIG. 2: Cross-resonance oscillation of target transmon Q_2 with the controlled transmon Q_1 in its ground state. (Left/Right panel) Population oscillation for target transmon Q_2 as a function of strength Ω_d of the driving applied on transmon Q_1 and time with parameter set (ω_c, g_{12}) marked with open circle/square shown in Figs. 2(c,d) of the main text. The other system parameters are similar to those used in Fig. 2 of the main text. The horizontal dashed lines indicates the driving strength $\Omega/2\pi = 10$ MHz that is used to infer the effective XY coupling strength J [4].

transmons $|002(200)\rangle$, respectively, and $J_{020}, J_{200(002)}$ denote the associated effective coupling strength, given as

$$\begin{aligned} J_{020} &\simeq \sqrt{2}g_{1c}g_{2c}\left(\frac{1}{\Delta_1} + \frac{1}{\Delta_2}\right) \simeq \frac{2\sqrt{2}g_{1c}g_{2c}}{\Delta}, \\ J_{200} &\simeq \sqrt{2}\left(g_{12} + \frac{g_{1c}g_{2c}}{\Delta_1}\right) \simeq \sqrt{2}J, \\ J_{002} &\simeq \sqrt{2}\left(g_{12} + \frac{g_{1c}g_{2c}}{\Delta_2}\right) \simeq \sqrt{2}J, \end{aligned} \quad (7)$$

while term ζ_1 results from the interaction among lower-energy states of qubits and coupler.

ESTIMATED XY COUPLING STRENGTH FROM CROSS-RESONANCE OSCILLATION

For two on-resonantly coupled qubits, the inter-qubit XY coupling strength can be extracted as half the energy difference between the eigenstate $|100\rangle$ and $|001\rangle$. However, for two off-resonant qubits coupled via a coupler circuit shown in Fig.1(b) of the main text, the effective XY coupling is not perfectly well-defined in this case. In present work, the XY coupling strength is estimated from the period T of the cross-resonance oscillation with the controlled qubit Q_1 in its ground state, as shown in Fig. 2. In the weak-drive limit, the period T of the oscillations can be well approximated by $2\pi/T = J\Omega_d/\Delta_{12}$ [4], where Ω_d denotes strength of the driving applied on Q_1 . In present work, $\Omega/2\pi = 10$ MHz is used to infer the XY coupling strength.

OFF-RESONANTLY COUPLED QUBITS WITH VARYING QUBIT DETUNING

As we have mentioned in the main text, the strength of the maintained XY coupling may further increase by optimizing the full system parameters. In Figs. 3 and 4, we

have shown the landscapes of XY coupling J and ZZ coupling ζ as a function of coupler frequency ω_c and direct coupling strength g_{12} for off-resonantly coupled qubits system with different qubit detuning, i.e., $\Delta_{12}/2\pi = 100$ MHz, and $\Delta_{12}/2\pi = 50$ MHz, respectively.

ON-RESONANTLY COUPLED QUBITS WITH VARYING COUPLER ANHARMONICITY

Similar to the off-resonantly coupled case, when we reduce the energy of $|020\rangle$, i.e., increasing the coupler anharmonicity for on-resonantly coupled transmon system, the negative ZZ contribution (ζ_{020}) from interaction $|101\rangle \leftrightarrow |020\rangle$ gets larger, thus a larger maintained XY coupling J is needed to suppress ZZ coupling. Figure 5 show the numerical calculated ZZ coupling strength and the XY coupling strength as a function of ω_c and g_{12} with coupler anharmonicity $\alpha_c/2\pi = \{0, -200, -400, -600\}$ MHz. The other parameters are same to those used in Fig. 4(a) of the main text. One can indeed find that the lower branch of zero- ZZ region is shifted downward along with the increased coupler anharmonicity, suggesting a larger maintained XY coupling.

TUNABLE COUPLING SUPERCONDUCTING CIRCUIT

In this section, we show that suppressing ZZ coupling while preserving XY coupling can also be realized in the qubit architecture proposed by P. S. Mundada *et al.* [5], where two transmons are coupled via a coupling circuit comprising two bus couplers. According to Ref. [5], the full system can be modeled as four coupled weakly anharmonic oscillators, and its Hamiltonian reads

$$\begin{aligned} H &= \sum_{j=1,2,\pm} (\tilde{\omega}_j q_j^\dagger q_j + \frac{\alpha_j}{2} q_j^\dagger q_j^\dagger q_j q_j) \\ &+ \sum_{\substack{j=1,2 \\ k=\pm}} g_{jk} (q_j q_k^\dagger + q_j^\dagger q_k), \end{aligned} \quad (8)$$

where subscript $j(k) = \{1, 2, \pm\}$ labels anharmonic oscillator Q_j with anharmonicity α_j and bare transition frequency $\tilde{\omega}_j$, q_j (q_j^\dagger) is the associated annihilation (creation) operator, and g_{jk} denotes strength of the coupling between Q_j and Q_k .

From second-order perturbation theory, the XY coupling strength can be obtained as

$$\begin{aligned} J &= J_+ + J_-, \\ J_\pm &= g_{1\pm}g_{2\pm}/\Delta_\pm, \end{aligned} \quad (9)$$

with $1/\Delta_\pm = (1/\Delta_{1\pm} + 1/\Delta_{2\pm})/2$. The ZZ coupling can be defined as $\zeta = (E_{1100} - E_{1000}) - (E_{0100} - E_{0000})$, where $E_{n_1 n_2 n_- n_+}$ denotes the energy of system eigenstate $|n_1 n_2 n_- n_+\rangle$ ($n_1, n_2, n_-, n_+ = \{0, 1, 2\}$). According to the fourth order perturbation theory [1, 5], the expression for ζ is $\zeta = \zeta_{2000} + \zeta_{0200} + \zeta_{0020} + \zeta_{0002} + \zeta_1$ with

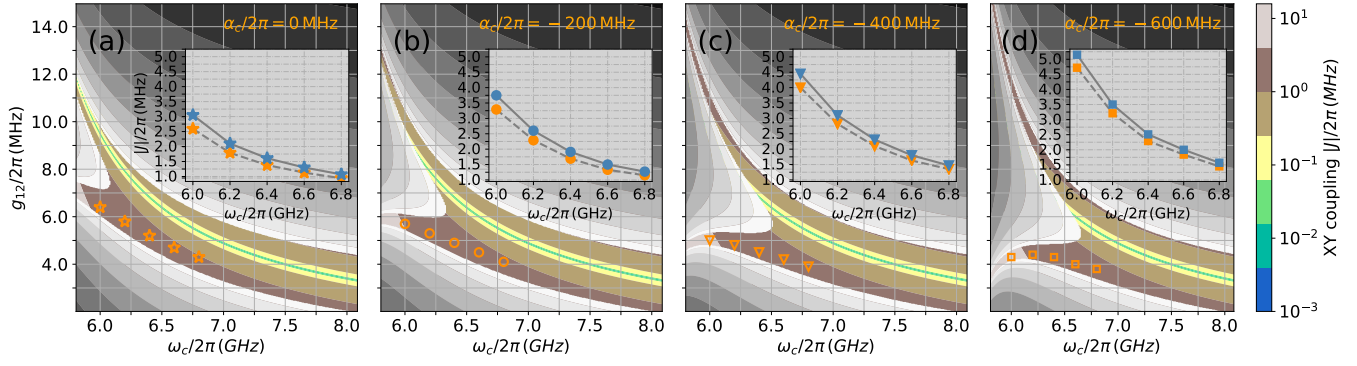


FIG. 3: Landscapes of XY coupling J and ZZ coupling ζ as a function of coupler frequency ω_c and direct coupling strength g_{12} with qubit frequency $\omega_{1(2)}/2\pi = 5.114$ (5.014) GHz. The other system parameters are similar to those used in Fig. 3 of the main text, where the qubit detuning $\Delta_{12}/2\pi = 200$ MHz. Here the two-qubit detuning $\Delta_{12}/2\pi = 100$ MHz.

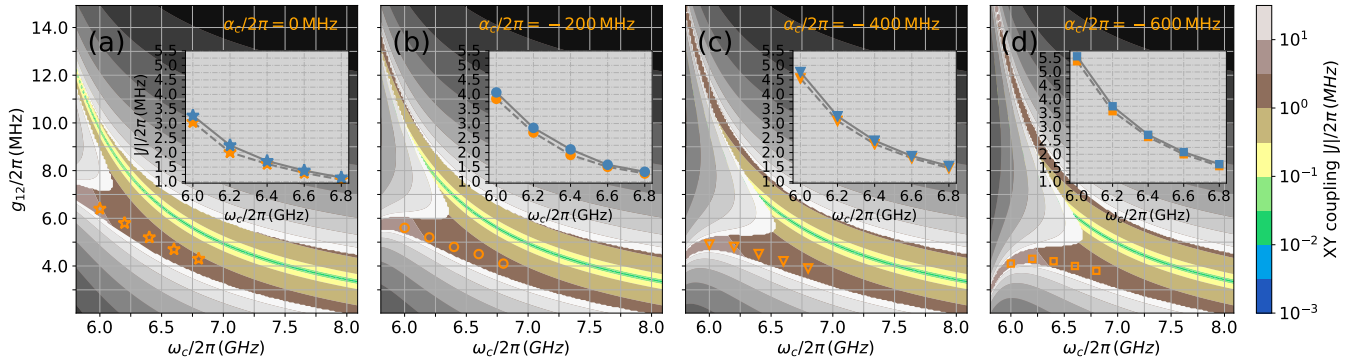


FIG. 4: Landscapes of XY coupling J and ZZ coupling ζ as a function of coupler frequency ω_c and direct coupling strength g_{12} with qubit frequency $\omega_{1(2)}/2\pi = 5.114$ (5.064) GHz. The other system parameters are similar to those used in Fig. 3 of the main text, where the qubit detuning $\Delta_{12}/2\pi = 200$ MHz. Here the two-qubit detuning $\Delta_{12}/2\pi = 50$ MHz.

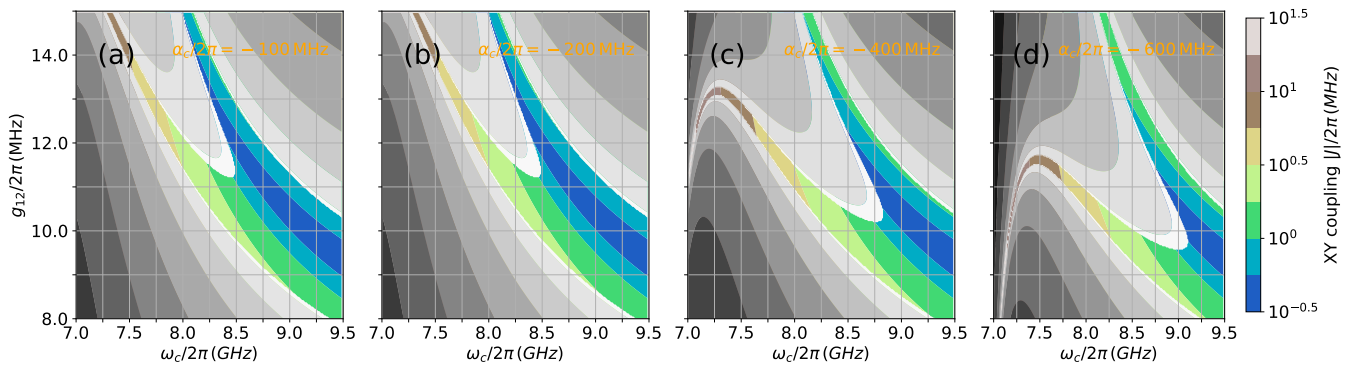


FIG. 5: Landscapes of XY coupling J and ZZ coupling ζ as a function of coupler frequency ω_c and direct coupling strength g_{12} for on-resonantly coupled qubits. (a) $\alpha_c/2\pi = 0$ (linear coupler), (b) $\alpha_c/2\pi = -200$ MHz, (c) $\alpha_c/2\pi = -400$ MHz (see also in Fig. 4(a) of the main text), and (d) $\alpha_c/2\pi = -600$ MHz. The other system parameters are similar to those used in Fig. 4(a) of the main text.

$$\begin{aligned}
\zeta_{2000} &= \left(\frac{g_{1+}g_{2+}}{\Delta_{2+}} + \frac{g_{1-}g_{2-}}{\Delta_{2-}} \right)^2 \left(\frac{2}{-\Delta_{12} - \alpha_1} \right) = \frac{J_{2000}^2}{-\Delta_{12} - \alpha_1}, \\
\zeta_{0200} &= \left(\frac{g_{1+}g_{2+}}{\Delta_{1+}} + \frac{g_{1-}g_{2-}}{\Delta_{1-}} \right)^2 \left(\frac{2}{\Delta_{12} - \alpha_2} \right) = \frac{J_{0200}^2}{\Delta_{12} - \alpha_2}, \\
\zeta_{0020} &= \frac{2g_{1+}^2g_{2+}^2}{\Delta_{1+} + \Delta_{2+} + \alpha_+} \left(\frac{1}{\Delta_{1+}} + \frac{1}{\Delta_{2+}} \right)^2 = \frac{J_{0020}^2}{\Delta_{1+} + \Delta_{2+} + \alpha_+}, \\
\zeta_{0002} &= \frac{2g_{1-}^2g_{2-}^2}{\Delta_{1-} + \Delta_{2-} + \alpha_-} \left(\frac{1}{\Delta_{1-}} + \frac{1}{\Delta_{2-}} \right)^2 = \frac{J_{0002}^2}{\Delta_{1-} + \Delta_{2-} + \alpha_-}, \\
\zeta_1 &= \frac{1}{\Delta_{12}} \left[\left(\frac{g_{1+}g_{2+}}{\Delta_{1+}} + \frac{g_{1-}g_{2-}}{\Delta_{1-}} \right)^2 - \left(\frac{g_{1+}g_{2+}}{\Delta_{2+}} + \frac{g_{1-}g_{2-}}{\Delta_{2-}} \right)^2 \right] \\
&\quad + \left[g_{1+}g_{2-} \left(\frac{1}{\Delta_{1+}} + \frac{1}{\Delta_{2-}} \right) + g_{1-}g_{2+} \left(\frac{1}{\Delta_{1-}} + \frac{1}{\Delta_{2+}} \right) \right]^2 \frac{1}{\Delta_{1+} + \Delta_{2-}} \\
&\quad - \left(\frac{g_{1+}^2}{\Delta_{1+}^2} + \frac{g_{1-}^2}{\Delta_{1-}^2} \right) \left(\frac{g_{2+}^2}{\Delta_{2+}^2} + \frac{g_{2-}^2}{\Delta_{2-}^2} \right) - \left(\frac{g_{2+}^2}{\Delta_{2+}^2} + \frac{g_{2-}^2}{\Delta_{2-}^2} \right) \left(\frac{g_{1+}^2}{\Delta_{1+}^2} + \frac{g_{1-}^2}{\Delta_{1-}^2} \right),
\end{aligned} \tag{10}$$

where $\Delta_{ij} = \tilde{\omega}_i - \tilde{\omega}_j$. The terms $\zeta_{2000(0200)}$ and $\zeta_{0020(0002)}$ can be considered as the ZZ contributions resulting from the effective coupling between qubit state $|1100\rangle$ and higher-energy states of transmons $|2000(0200)\rangle$ and coupled $|0020(0002)\rangle$, respectively, and the associated effective coupling strength can be approximated as

$$\begin{aligned}
J_{2000} &\simeq \sqrt{2}J, J_{0200} \simeq \sqrt{2}J, \\
J_{0020} &\simeq 2\sqrt{2}J_+, J_{0002} \simeq 2\sqrt{2}J_-,
\end{aligned} \tag{11}$$

while term ζ_1 results from the interaction among lower-energy states of qubits and coupler.

From Eqs. (9), (10) and (11), one can find that the conditions for achieving zero- XY coupling and zero- ZZ coupling is not coexist in the same parameter space. This suggests that in this coupler architecture, one may suppress static ZZ coupling while preserve XY interaction. In Figs. 6, 7, and 8, we demonstrate numerically that in this architecture, the static ZZ coupling can indeed be heavily suppressed without the need for suppressing XY coupling. Thus, XY -based two-qubit gates could be implemented without the detrimental ef-

fect from static ZZ coupling.

* Electronic address: shangniguo@sina.com

† Electronic address: land@nju.edu.cn

‡ Electronic address: tanxs@nju.edu.cn

- [1] R. Krishnan and J. A. Pople, Approximate fourth-order perturbation theory of the electron correlation energy, *Int. J. Quantum Chem.* **14**, 91 (1978).
- [2] X. Li, T. Cai, H. Yan, Z. Wang, X. Pan, Y. Ma, W. Cai, J. Han, Z. Hua, X. Han, Y. Wu, H. Zhang, H. Wang, Yipu Song, Luming Duan, and Luyan Sun, Tunable Coupler for Realizing a Controlled-Phase Gate with Dynamically Decoupled Regime in a Superconducting Circuit, *Phys. Rev. Applied* **14**, 024070 (2020).
- [3] J. Chu *et al.*, in preparation. (2020).
- [4] E. Magesan and J. M. Gambetta, Effective Hamiltonian models of the cross-resonance gate, *Phys. Rev. A* **101**, 052308 (2020).
- [5] P. S. Mundada, G. Zhang, T. Hazard, and A. A. Houck, Suppression of Qubit Crosstalk in a Tunable Coupling Superconducting Circuit, *Phys. Rev. Applied* **12**, 054023 (2019).

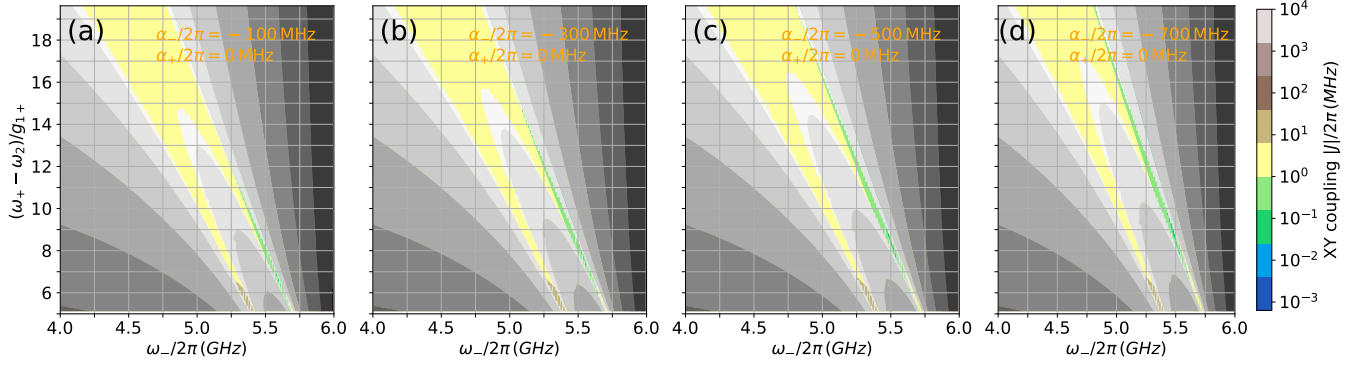


FIG. 6: Off-resonance case. Landscapes of XY coupling J (perturbation theory) and ZZ coupling ζ (numerical diagonalization) as a function of coupler frequency ω_{\pm} with qubit frequency $\omega_{1(2)}/2\pi = 6.143$ (6.421) GHz, qubit anharmonicity $\alpha_{1(2)}/2\pi = -330$ MHz, coupler anharmonicity $\alpha_{+}/2\pi = 0$ MHz, transmon-coupler coupling strength $g_{1-(2-)} / 2\pi = 85$ MHz, $g_{1+(2+)} / 2\pi = 102$ MHz [5] and coupler anharmonicity (a) $\alpha_{-}/2\pi = -100$ MHz, (b) $\alpha_{-}/2\pi = -300$ MHz, (c) $\alpha_{-}/2\pi = -500$ MHz, and (d) $\alpha_{-}/2\pi = -700$ MHz. For each coupler anharmonicity, the two landscapes are shown in single panel, and the data point in the landscape of ZZ coupling with ζ below 20 KHz is removed.

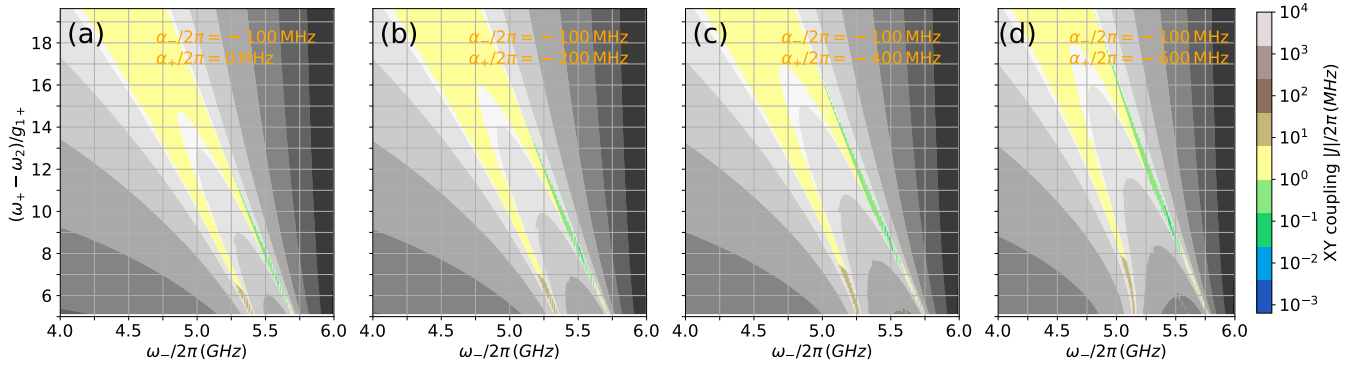


FIG. 7: Off-resonance case. Landscapes of XY coupling J (perturbation theory) and ZZ coupling ζ (numerical diagonalization) as a function of coupler frequency ω_{\pm} with coupler anharmonicity $\alpha_{-}/2\pi = -100$ MHz. (a) $\alpha_{+}/2\pi = 0$, (b) $\alpha_{+}/2\pi = -200$ MHz, (c) $\alpha_{+}/2\pi = -400$ MHz, and (d) $\alpha_{+}/2\pi = -600$ MHz. The other system parameters are similar to those used in Fig. 6.

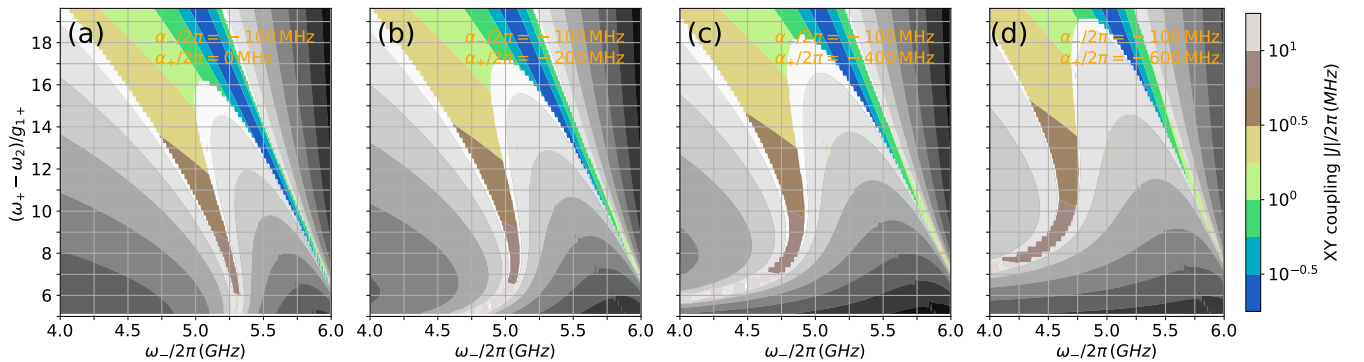


FIG. 8: On-resonance case. Landscapes of XY coupling J (numerical diagonalization) and ZZ coupling ζ (numerical diagonalization) as a function of coupler frequency ω_{\pm} with qubit frequency $\omega_{1(2)}/2\pi = 6.421$ GHz. The other system parameters are similar to those used in Fig. 7.

